Binding of a Brownian nanoparticle to a thermally fluctuating membrane surface

Hsueh-Te Chung and Hsiu-Yu Yu ⬤[*]

Department of Chemical Engineering, National Taiwan University, Taipei 10617, Taiwan

We investigate the Brownian dynamics of a nanoparticle bound to a thermally undulating elastic membrane. The ligand-functionalized nanoparticle is assumed to interact monovalently with the receptor expressed on the membrane. In order to resolve the nanoparticle transient motion subject to the instantaneous membrane configuration in a consistent manner, we employ a set of coupled Langevin equations that simultaneously incorporate the hydrodynamic effects, ligand-receptor binding interaction, intramembrane elastic forces, and thermal fluctuations. We show that the presence of a deformable, elastic fluid membrane not only affects the dynamics of a bound nanoparticle but also alters the effective binding potential felt by the nanoparticle. In contrast to a nanoparticle bound to a flat surface, the oscillatory characteristics of the nanoparticle velocity autocorrelation function are suppressed and transition to an anticorrelated long-time tail. Moreover, the nanoparticle position fluctuation becomes more coherent with that of the membrane binding site, and the width of the distribution of the nanoparticle distance from the membrane decreases with increasing membrane bending rigidity. By introducing a locally harmonic, bistable potential as an effective potential for the ligand-receptor pair, the rate of nanoparticle transitioning between two bound states is facilitated by membrane undulations as a result of stronger positional variations associated with the nanoparticle.

I. INTRODUCTION

In soft matter applications involving biological membranes, the membrane shape and dynamics simultaneously impact the local fluid environment. The membrane surface configuration defines the boundary condition of the fluid, and temperature-induced fluctuations (i.e., thermal or Brownian effects) make the fluid-bounding surface change with time. As a result, such "membrane-mediated" hydrodynamic interactions take part in processes such as nanoparticle or nanomaterial binding to cells [1–3], biosensing [4,5], endocytosis or internalization [6,7], and cell adhesion [8,9]. In these examples, aside from the essential binding interactions involved, the intervening fluid force set up by the instantaneous boundary conditions also impact the associated dynamics. In this work, we consider a ligand-functionalized nanoparticle, known as nanocarrier (NC) in vascular targeted drug delivery [10–13], as an example, and provide consistent theoretical descriptions for configurations of both the nanoparticle and the interacting receptor-expressing fluid membrane using the framework of Langevin equations. Given the assumed monovalent binding between the ligand and receptor, a minimal set of equations for the interacting NC-membrane system enable a rational exploration into the coupled dynamics of a bound Brownian particle and a thermally fluctuating membrane.

Cellular membranes have unique local shapes as a result of intrinsic elastic properties and interactions between constituting lipids and proteins in the presence of the surrounding fluid. For example, in receptor-mediated endocytosis, clathrin on the membrane forms a cage structure that facilitates the formation of a vesicle. Such deformations of membranes play a critical role in transporting NCs from the extracellular matrix to the cytosol [14,15]. Meanwhile, some proteins embedded in the lipid matrix induce curvatures that enable cellular membranes to exhibit various shapes including plane, cylinder, saddle, and sphere [16]. Theoretically, the Helfrich model [17] for the elastic energy is widely employed to describe the conformation of a continuous, two-dimensional fluid membrane, where the membrane Hamiltonian is determined by the intrinsic properties such as the bending rigidity, splay modulus, and tension. Making use of this description, various shapes of biological membranes are successfully predicted [16], and the energy states of membranes are quantified as a function of the extent of deformation [18]. While typical lipid bilayers are several nanometers thick, as long as the overall dimension of the membrane in width is much larger than $O(\text{nm})$, it is expected that the Helfrich-type, elastic description is applicable for describing the shape variation of a homogeneous membrane. For membranes that are heterogeneous in curvature and mechanical properties, generalization of the standard Helfrich model for multicomponent membranes may be pursued [19].

The interaction between colloids and membranes has been an active research area owing to its prominence in the applications outlined above. Within the framework of the Helfrich Hamiltonian, the deformation of a fluid membrane as a result of a bound and wrapped particle has been analyzed theoretically [20–22]. Making use of coarse-grained molecular dynamics simulations, the dynamical barrier of nanoparticle internalization is qualitatively demonstrated [23,24]. From the perspective of the system free energy minimum, Monte Carlo (MC) simulations for triangulated membranes have been used to explore the nanoparticle-membrane configurational space, and predicted the paths for internalization [25], aggregation of

*hsiuyuyu@ntu.edu.tw

nanoparticles [26], and membrane tubulation [27]. In a recent study for NC binding mediated by receptor-ligand interactions, MC simulations have shown that the energy state of the membrane is strongly coupled to the configurational entropy of the NC, and the binding potential of mean force (PMF) has been identified for multivalent ligand-receptor bonds [13]. It has also been shown simultaneously by experiment and MC simulations that attraction between Brownian particles can be mediated by a deformed membrane [28]. While these MC efforts provide a promising theoretical basis for nanoparticle-cell interactions from the viewpoint of equilibrium thermodynamics, the temporal response of a bound nanoparticle over the fluid inertial regime is inaccessible.

Near fluid membranes, the motion of a nanoparticle is hindered due to the enhanced hydrodynamic resistance on the particle. Moreover, the presence of a bounding interface breaks the symmetry of the fluid domain, making the particle mobility anisotropic. Various treatments for the interface have lead to predictions for the particle mobility with different levels of details. In the simplest assumption, the reduced mobility (or enhanced drag) of the particle near a membrane can be approximated as that near a solid wall [29–32]. In order to capture the deformation of fluid membranes, more detailed considerations such as a particle near a fluid-fluid interface [33–36] or a particle near an elastic interface [37–41] may be applied. In fact, the back flow as a result of the deformed membrane has been shown to create memory effects on particle diffusion, and the associated time-dependent mobility tensor in the zero-frequency limit is found to reduce to the universal result for a particle moving near a no-slip solid wall [38,40]. Making use of the generalized Langevin equation framework and direct numerical simulations, the hydrodynamics and thermal effects for a nanoparticle adhered to the endothelium via monovalent ligand-receptor interaction have been characterized without considering membrane deformation [42,43]. In these studies, it has been demonstrated that once the added mass resulted from the fluid inertia is consistently taken into account, the temporal decays of the velocity autorrelations for a bound nanoparticle without considering the time-dependent hydrodynamic resistance agree reasonably well with those in the presence of full hydrodynamic relaxation spectrum. Such a similarity has been attributed to both the near-wall enhanced hydrodynamic resistance and the strong binding force between the ligand-receptor pair. Adopting the same argument, under quasiequilibrium assumption for membrane undulations, the membrane-mediated ligand-receptor binding potential has been considered in a more recent study of a polymer-grafted nanoparticle from a purely thermodynamic standpoint [44], where it has been suggested that the distribution of the nanoparticle relative to the interacting surface is altered in the presence of the membrane-mediated softened potential.

If the membrane is thermally undulating, then its instantaneous conformation yields variation in the perpendicular position of anchored receptors, which further impacts the motion of the interacting ligand-functionalized nanoparticle. In the presence of small deformations, in a Monge gauge the time-dependent local membrane height can be described by a Langevin equation (LE) with the Oseen tensor representing the viscous effect between a given pair of membrane elements [45]. Such a framework has been realized through stochastic simulations in Fourier space that incorporate the local elastic force on the membrane element defined by the Helfrich Hamiltonian [46]. The Fourier space Brownian dynamics (FSBD) algorithm efficiently integrates the equation of motion for the amplitudes of the membrane Fourier modes, and can achieve relatively longer simulation timescale and larger simulation length scale. This algorithm has been implemented to study membrane configurations with cytoskeletal interactions [47], protein diffusion on undulating membranes [48–50], as well as receptor-mediated adhesion between a fluctuating membrane and an elastic substrate [51,52], provided the assumption of a constant effective bending rigidity is valid.

In order to make one step forward to incorporate thermal undulations of membrane surfaces in the dynamical modeling of receptor-mediated binding of a ligand-functionalized nanoparticle over the fluid inertial regime, in this work, we formulate a set of coupled stochastic equations for a bound NC and an interacting membrane surface shown in Fig. 1. Instead of performing a time-Fourier analysis of the time-dependent mobility tensor for the velocity autocorrelation function (ACF) [38,40,41], for purposes of instantaneous tracking of particle trajectory in the presence of Brownian effects, the stochastic motion of the nanoparticle center of mass is described using a LE with the added mass included and an accordingly modified instantaneous drag coefficient representing the near-cell lubrication force, whereas the thermal fluctuations of tension-free interacting membrane elements are simulated through FSBD. In the presence of only monovalent binding between the NC and membrane mediated by a pair of rigid ligand and receptor, we focus on one-dimensional Brownian motion of the NC perpendicular to the average membrane surface. In this manner, we neglect the flexure rigidity of both the receptor and ligand, and omit the effects of lateral diffusion of membrane elements and anchored receptor proteins. The binding energy between the ligand–receptor pair is assumed to be locally harmonic along the one-dimensional reaction coordinate with varying force constant. Such simple shape of the potential approximates the actual ligand-receptor interaction in biophysically relevant conditions [11]. Through simultaneous time integration of the two equations (LE and FSBD), we simulate the real-time stochastic motion of the NC and realize the instantaneous membrane undulations in the Fourier space. We analyze the resulting trajectories for the NC and membrane elements through ensemble averaging, and obtain the temporal decays of the NC velocity, NC position, and the membrane height given prescribed equilibrium states through ACF. Additionally, in order to evaluate the effect of membrane thermal undulations on the NC binding, we examine the distributions of ligand-receptor separation as well as our chosen order parameter that quantifies the distance between the centers of mass for NC and interacting membrane elements, respectively. Finally, we modify the simple harmonic binding potential to a bistable potential mimicking the effective one-dimensional energy landscape of two bound states, and allow the NC to explore its conformational space among the two basins. Analyzing how the flux of the particle trajectories pass over the barrier [53], we quantify the variation of the rates for NC to transition between the two
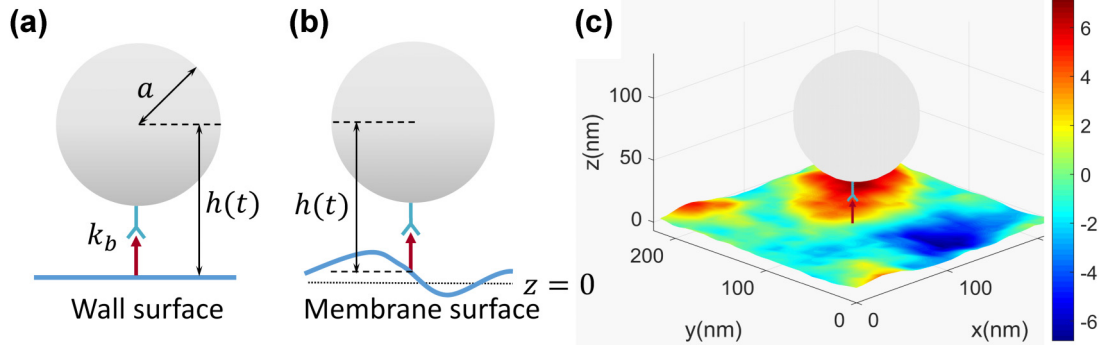
FIG. 1. (a) Schematic for an NC of radius a bound to a flat surface via monovalent ligand-receptor interaction and (b) the corresponding schematic for an NC bound to an undulating membrane. The solid blue wavy curve is the membrane surface, the horizontal dotted line denotes the initial equilibrium position of the membrane center of mass $z = 0$, and $h(t)$ is the instantaneous separation between the NC center of mass and the tethering position of the interacting receptor on membrane. (c) Simulation snapshot for the NC-membrane system with $K_c = 20\,k_B T$. The bound NC is shown in light gray and the out-of-plane fluctuations of membrane elements relative to $z = 0$ are shown with the color scale defined by the color bar in units of nanometers.

prescribed bound states in the presence of membrane thermal undulations.

The remaining part of the paper is organized as follows. In Sec. II, we first introduce our theory for the coupled NC-membrane motion. The details of the numerical method and parameter determination are presented in Sec. III followed by the discussion of the analyzed results in Sec. IV, where we separately present our predictions for the dynamics of an NC bound to a flat substrate and a fluctuating membrane (Sec. IV A), and assess the corresponding impact on the binding kinetics (Sec. IV B). Finally, we conclude our findings in Sec. V.

II. Theoretical model

In targeted drug delivery applications, the nanoparticle is surface-covered by polymeric and charged biomolecules with multiple binding sites [54–56]. The targeted membrane has multiple mobile receptor proteins whose diffusion and distribution on membrane may also alter the local membrane properties [57,58]. Therefore, the nanoparticle may interact with a neighboring nanoparticle and recruit more receptors to facilitate multivalent binding [59–61]. Such complex interplay is expected to change the membrane local elastic properties such as the bending rigidity and spontaneous curvature as a result of the changes in the distribution and composition of lipids as well as the structural transition of lipids due to electrostatic or ligand-receptor mediated interactions. Moreover, hydrodynamic interactions for multiple particles near a bounding surface bring in additional complexity owing to the induced and coupled relaxation timescales for the interacting particles mediated by the surface. All of these effects make the NC-membrane binding a multiscale and multiphysics problem; different levels of details would require distinct assumptions to be resolved simultaneously and truthfully. In this study, in order to first scrutinize how the dynamical relaxation of a bound NC is impacted by a thermally fluctuating surface using a tractable Langevin framework, we consider a much simplified scenario where both the nanoparticle and membrane receptor are in their dilute conditions such that

over the timescale of interest (namely, hydrodynamic regime) only a single nanoparticle is monovalently attached to the membrane surface.

The schematic of our model system is illustrated in Fig. 1. The system is separated by a membrane into the extracellular space and the cytoplasm. The ligand-functionalized NC modeled as a hard sphere of radius a and mass m_p is located at the extracellular side and interacts with the receptor-expressing membrane via ligand-receptor recognition denoted as the "harpoon-arrow pair" in the figure. In one dimension, the center of mass for the membrane surface is fixed at $z = 0$ and the center of mass for the bound NC is initially located at h_0 above the membrane binding site (tethering point of receptor). If both the ligand and receptor are considered as rigid with L_{ligand} and L_R being the lengths of the ligand and receptor, respectively, then $h_0 = a + L_{\text{ligand}} + L_R$ for an NC at its equilibrium bound state. For the coupled NC-membrane system, we separately formulate the equations for the out-of-plane displacements of membrane elements denoted as $z(\mathbf{r})$ and the displacement of NC center of mass relative to its initial height denoted as z_p.

We consider a membrane patch with its linear dimension L smaller than the length scale over which the membrane topology changes macroscopically but large enough for the short wavelength undulations to be captured truthfully. In the absence of curvature-inducing proteins and pinning effects, the elastic energy of the membrane under small deformations is determined by the Helfrich Hamiltonian in a Monge gauge [62]

$$E = \int_{\mathcal{A}} \left\{ \frac{K_c}{2} [\nabla^2 z(\mathbf{r})]^2 + \frac{\sigma}{2} [\nabla z(\mathbf{r})]^2 \right\} d\mathbf{r}, \qquad (1)$$

where the first term characterizes the effect of local mean curvature with K_c being the effective bending rigidity and the second term denotes the contribution from the membrane tension σ. $\mathcal{A} = L^2$ is the projected area of the two-dimensional square patch, and $z(\mathbf{r}) = z(x, y)$ is the height of the membrane element located at $\mathbf{r}$ in the xy plane ($z = 0$). In most physiological conditions the effect of membrane tension is small [47,62], and the second term in the integral can be

omitted. In addition, an external binding energy term E_b due to the adhered NC should be considered in the Hamiltonian. For rigid ligand and receptor, their specific interaction directly contributes to E_b. We model the binding potential between a given pair of ligand and receptor as harmonic [42,44,63] of the form,

$$E_b = \int_{\mathcal{A}} \frac{1}{2} k_b d^2 \delta(\mathbf{r}) d\mathbf{r}, \qquad (2)$$

where k_b is the harmonic force constant, $d = z_p - z_m$ is the separation between the tips of interacting ligand and receptor with z_m being the displacement of the membrane binding site relative its initial height when the nanoparticle is bound, and $\delta(\mathbf{r})$ is the Dirac delta function fixing the tethered receptor to the center of the membrane patch.

At a low Reynolds number with small out-of-plane fluctuations, each membrane element can be hydrodynamically viewed as a point particle in space. The velocity of a point particle at $\mathbf{r}$ would be linearly dependent on the force acting on another distant particle at $\mathbf{r}'$. In the continuum limit where the membrane elements are connected by the intrinsic elastic force, the equation of motion for the membrane patch is formulated as a nonlocal Brownian dynamics equation [45,46]

$$\frac{\partial z(\mathbf{r}, t)}{\partial t} = \int_{-\infty}^{\infty} \Lambda(\mathbf{r}, \mathbf{r}')[F(\mathbf{r}', t) + F_b(\mathbf{r}', t) + \zeta(\mathbf{r}', t)] d\mathbf{r}', \qquad (3)$$

where $F(\mathbf{r}, t) = -\frac{\delta E}{\delta z(\mathbf{r}, t)} = -K_c \nabla^4 z(\mathbf{r}, t) - \sigma \nabla^2 z(\mathbf{r}, t)$ is the membrane elastic force per unit area and $F_b(\mathbf{r}, t) = -\frac{\delta E_b}{\delta z(\mathbf{r}, t)} = -k_b[z_m(t) - z_p(t)]\delta(\mathbf{r})$ exerting on the binding site. As the membrane is bound to the NC at a single binding site with their closest separation to be of $O(30 \text{ nm})$ (typical size of an antigen-antibody pair [11]), we may generally view the membrane as unconfined. Therefore, we express $\Lambda(\mathbf{r}, \mathbf{r}') = \frac{1}{8\pi\eta|\mathbf{r} - \mathbf{r}'|}$, which is the diagonal part of the Oseen tensor in the free-particle limit with η being the viscosity of the surrounding fluid. $\zeta(\mathbf{r}, t)$ denotes the thermal fluctuating force that satisfies the fluctuation-dissipation theorem [64]:

$$\langle \zeta(\mathbf{r}, t) \rangle = 0$$
$$\langle \zeta(\mathbf{r}, t) \zeta(\mathbf{r}', t') \rangle = 2k_B T \Lambda^{-1}(\mathbf{r}, \mathbf{r}') \delta(t - t'), \qquad (4)$$

where $\Lambda^{-1}(\mathbf{r})$ is defined by $\int_{-\infty}^{\infty} \Lambda(\mathbf{r}, \mathbf{r}')\Lambda^{-1}(\mathbf{r}) d\mathbf{r}' = \delta(\mathbf{r})$, k_B is the Boltzmann constant, and T is the temperature. As the NC is modeled effectively as a hard sphere and the membrane out-of-plane deformations are considered as small, the short-range repulsive interactions [52] between the surfaces of NC and membrane are neglected here. If necessary, these forces can be added to Eq. (3) in a straightforward way.

The convolution integral in Eq. (3) can be efficiently managed in Fourier space. Therefore, making use of the Fourier transform

$$z_{\mathbf{k}} = \int_{\mathcal{A}} z(\mathbf{r}) e^{-i\mathbf{k} \cdot \mathbf{r}} d\mathbf{r} \qquad (5)$$

and the corresponding inversion

$$z(\mathbf{r}) = \frac{1}{L^2} \sum_{\mathbf{k}} z_{\mathbf{k}} e^{i\mathbf{k} \cdot \mathbf{r}}, \qquad (6)$$

we arrive at the following FSBD equation,

$$\frac{\partial z_{\mathbf{k}}}{\partial t} = \Lambda_{\mathbf{k}}[F_{\mathbf{k}}(t) + F_{b,\mathbf{k}}(t) + \zeta_{\mathbf{k}}(t)], \qquad (7)$$

where $\mathbf{k}$ is the wave vector, $\Lambda_{\mathbf{k}} = 1/(4\eta k)$, $F_{\mathbf{k}} = -K_c k^4 z_{\mathbf{k}}$ for zero tension ($\sigma = 0$), $F_{b,\mathbf{k}} = -k_b[z_m(t) - z_p(t)]$ applying on all $\mathbf{k}$, and $\zeta_{\mathbf{k}}$ satisfies

$$\langle \zeta_{\mathbf{k}}(t) \rangle = 0$$
$$\langle \zeta_{\mathbf{k}}(t) \zeta_{\mathbf{k}'}(t') \rangle = 2k_B T L^2 \Lambda_{\mathbf{k}}^{-1} \delta_{\mathbf{k}, -\mathbf{k}'} \delta(t - t'). \qquad (8)$$

In the limit of large L, the variation in the membrane center of mass position is negligible, and we may directly set $\Lambda_{\mathbf{k}=0} = 0$ to avoid the divergence in $\Lambda_{\mathbf{k}} = 1/(4\eta k)$ [46,47].

Simultaneously, the NC undergoes a restrained Brownian motion subjected to the monovalent ligand-receptor bond. Close to the bounding surface, the hydrodynamic resistance would be augmented by a factor dependent on the instantaneous separation between the NC and membrane. As noted in Sec. I, the particle mobility near a membrane reduces to the value near a no-slip solid surface in the zero-frequency limit [38,40], and at the same time the temporal decay of the velocity for a bound particle can be approximately predicted by considering only a time-independent hydrodynamic resistance with an increased effective particle mass [42,43]. At the same level of quasisteady assumption for the lubrication force on the particle, we therefore formulate the NC equation of motion in terms of a Langevin equation that reads

$$M \frac{d^2 z_p}{dt^2} = -\frac{6\pi\mu a^2}{[h(t) - a]} \frac{dz_p}{dt} - k_b[z_p(t) - z_m(t)] + R(t), \qquad (9)$$

where $M = m_p + \frac{1}{2}m_p = \frac{3}{2}m_p$ is the effective mass of the NC if treated as neutrally buoyant with $\frac{1}{2}m_p$ being the added mass and $\frac{dz_p}{dt} = v(t)$ is the NC velocity in the z direction. On the right-hand side, the first term denotes the hydrodynamic drag force which is simply a Stokes drag times an enhancement factor accounting for the near-surface lubrication effect [32] with $h(t)$ being the instantaneous separation between the NC center of mass and the membrane reference position [see Fig. 1(b)]. Under small membrane deformations, we choose the reference position to be the height of the binding site such that $h(t) = z_p(t) + h_0 - z_m(t)$. The second term on the right-hand side is the binding force, and $R(t)$ is the Brownian force on the NC again obeying the fluctuation-dissipation relation [64]:

$$\langle R(t) \rangle = 0$$
$$\langle R(t) R(t') \rangle = \frac{12\pi\mu a^2 k_B T}{[h(t) - a]} \delta(t - t'). \qquad (10)$$

The two coupled stochastic equations [Eqs. (7) and (9)] are integrated numerically to resolve the membrane fluctuations and NC binding dynamics, as detailed in the coming section.

III. SIMULATION METHOD AND ANALYSIS

The system considered is fixed at $T = 310$ K, the body temperature. The membrane patch is mapped on a square area of $L \times L$ composed of $N \times N$ equally spaced lattices of spacing $\ell = L/N$. In Fourier space, the wave vector $\mathbf{k}$

is defined by $\mathbf{k} = (m, n) \times 2\pi/L$, where m and n are integers ranging from $-(N/2) + 1$ to $N/2$. Periodic boundary conditions are imposed in both x and y directions so L is chosen to be large enough to eliminate size effects. In our simulations, we choose $\ell = 7$ nm, consistent with the lattice length in Refs. [46,47]. For the NC-membrane coupled system, we choose $L = 224$ nm, $N = 32$, $\eta = 0.0035$ Pa s (average of cytoplasm and water), and $K_c = 20$ or 50 $k_B T$, relevant for physiological endothelial cells in targeted drug delivery [13,62]. The smallest membrane relaxation time is then estimated as $\tau_m = 4\eta\ell^3/K_c(2\pi)^3 \sim 10^{-10}$ s. We have justified the choice of the system size by changing L to be 336 nm, and the results remain statistically unchanged (see the Supplemental Material [65]).

The nanoparticle is neutrally buoyant with a radius of 50 nm, chosen consistent with the size of NC in experiments [11,13]. The surrounding extracellular fluid is assumed to be waterlike with viscosity $\mu = 10^{-3}$ kg m^{-1} s^{-1} and density $\rho = 10^3$ kg/m^3. In order to consider parameters relevant for targeted endothelial cells expressed with intracellular adhesion molecule-1 (ICAM-1), we assume $L_{ligand} = 15$ nm for the ligand (antibody; anti-ICAM-1) and $L_R = 19$ nm for the receptor (antigen; ICAM-1) with the binding constant being $k_b = 1$ N/m [11]. Nevertheless, k_b may be generally considered as an adjustable force constant for a locally harmonic potential. On this basis, the equilibrium height of the nanoparticle is $h_0 = 84$ nm and we determine the intrinsic hydrodynamic viscous relaxation time (timescale for fluid momentum to diffuse over a) as $\tau_v = a^2\rho/\mu = 2.5 \times 10^{-9}$ s, the near-wall Brownian relaxation time (timescale over which the velocity correlations for the particle start to decay) as $\tau_B = M(h_0 - a)/6\pi\mu a^2 = 5.7 \times 10^{-10}$ s, and the harmonic-spring oscillation time $\tau_k = 2\pi\sqrt{M/k_b} = 5.6 \times 10^{-9}$ s.

The simulation is performed in a two-stage process to ensure that the membrane can reach equilibrium before interacting with the NC. In stage 1, the membrane is initially considered as a flat sheet with $z(\mathbf{r}) = 0$ and evolves according to Eq. (7) (omitting the term of F_b). We employ a forward Euler scheme with discrete Fourier transform adapted from Ref. [47] for all wave vectors to integrate Eq. (7) in time with step size Δt_1 and number of steps N_1. In stage 2, an NC is bound to the membrane and placed to h_0 above the center of membrane patch (the binding site) with $\frac{dz_p}{dt} = 0$ (zero initial velocity), and Eq. (9) is integrated simultaneously with Eq. (7) using finite difference scheme [42]. The step size is Δt_2 and the number of steps is N_2 for stage 2. For the coupled NC-membrane system, once the membrane Fourier modes are resolved at a given time t, inverse Fourier transform [Eq. (6)] leads to the out-of-plane displacement of the binding site z_m in Eq. (9), and the NC position is updated in real space accordingly at $t + \Delta t_2$. The updated NC position determines $F_{b,\mathbf{k}}$ in Eq. (7), allowing the evolution of membrane undulation modes to $t + \Delta t_2$. The procedure is repeated throughout stage 2. The stochastic forces for both NC and membrane modes are sampled from a Gaussian distribution with a zero mean and desired variances according to Eqs. (8) and (10). A representative simulation configuration is shown in Fig. 1(c) for $K_c = 20$ $k_B T$.

The step size is determined to be smaller than all the characteristic timescales of the system, and the number of steps is chosen to be large enough to ensure complete relaxation of the system and satisfactory statistics of the results. The following parameters are used in the majority of the dynamical simulations unless otherwise stated. For the NC-membrane system, at stage 1 we choose $\Delta t_1 = 10^{-9}$ s and $N_1 = 5 \times 10^7$ for $K_c = 20$ $k_B T$, and $\Delta t_1 = 10^{-10}$ s and $N_1 = 2 \times 10^8$ for $K_c = 50$ $k_B T$. At stage 2, $\Delta t_2 = 2 \times 10^{-11}$ s and $N_2 = 5 \times 10^8$ for both $K_c = 20$ $k_B T$ and 50 $k_B T$.

In stochastic simulations, the transient response of the system is monitored by calculating the ACF. For a physical quantity $A(t)$, its normalized autocorrelation function is defined by $C_A(t) = \langle A(t)A(0) \rangle / \langle A(0)^2 \rangle$ with $\langle \cdot \rangle$ being the ensemble average. ACF provides information of how the quantity $A(t)$ is correlated with its initial condition over time. We calculate the normalized velocity autocorrelation function (VACF) $[C_v(t) = \langle v(t)v(0) \rangle / \langle v(0)^2 \rangle]$ and the normalized position autocorrelation function (PACF) $[C_{z_p} = \langle z_p(t)z_p(0) \rangle / \langle z_p(0)^2 \rangle]$ of the NC to characterize how the NC responds to various forces in its inertial regime. Simultaneously, we compare the normalized membrane height autocorrelation function (HACF) of the central point (i.e., binding site) $[C_z(t) = \langle z(t)z(0) \rangle / \langle z(0)^2 \rangle]$ to determine how its temporal decay is affected by NC binding. We define two parameters to characterize the binding PMF: One is the direct separation between the ligand and receptor, d, and the other is the relative displacement between the NC center of mass (z_p) and the center of mass of membrane elements ($z_{c.m.}$) falling withing $2a$ from the NC center of mass (c.m.), $\Delta R = z_p - z_{c.m.}$. We calculate the distribution functions of both d and ΔR to characterize the membrane-mediated PMF for NC from different perspectives. All the ensemble averages are performed according to the standard techniques [66]. For NC dynamics, we save NC position and velocity every step and the ACFs and distribution functions are taken from 1000 to 5000 trajectories of 10^5 steps at stage 2; for membrane dynamics, for both stages, we save membrane configurations every 1000 steps and all the averaged quantities are calculated from these configurations. For clarity, the ACFs reported in log-log plots are magnitudes (absolute values) of the functions, and the unit of time is chosen to be the intrinsic hydrodynamic timescale, τ_v.

In order to validate our membrane simulation protocols, we have implemented the free membrane modeling for a red-blood-cell-like system with $\eta = 0.006$ Pa s (for cytoplasm viscosity) and a bending rigidity $K_c = 5$ $k_B T$ at 310 K [46,47]. The resulting dynamical correlation function (HACF) as well as the long-time configurations analyzed in both real space and Fourier space are consistent with the analytical theories for a tension-free and force-free membrane at thermal equilibrium (see Fig. S1 of the Supplemental Material [65]). Experimentally, depending on the desired spatial-temporal resolution, these properties can be measured using techniques such as flicker spectroscopy [67], dynamic optical displacement spectroscopy [67], reflection interference contrast microscopy [68] or time resolved membrane fluctuation spectroscopy [69,70]. In terms of nanoparticle dynamics, we have also performed LE simulations for a nanoparticle bound to a flat wall, and confirmed that the nanoparticle center-of-mass statistics satisfy the Maxwell-Boltzmann distribution function for velocity as well as the Boltzmann distribution function for position (see Fig. S3). In order to further check the

consistency of the stochastic simulations, the complementary deterministic simulations of the nanoparticle motion have been employed, where the nanoparticle is driven initially by an impulsive force which yields $v(0)$ without subsequent random fluctuations [$R(t > 0) = 0$ in Eq. (9)] [42–44]. The impulse has a Gaussian distribution with a variance defined by the preset temperature. For the flat wall system, the velocity temporal decay of the nanoparticle is directly reported. For the membrane system, we start the deterministic modeling for a given membrane configuration in stage 2. Once an NC is bound to it, an impulse is applied to the NC. We then simultaneously resolve the NC motion and membrane response according to Eqs. (9) and (7) in the absence of $R(t)$ and $\zeta(t)$. The normalized velocity response function, $v(t)/v(0)$, for both systems are determined along with the corresponding ensemble averaged VACFs.

IV. RESULTS AND DISCUSSION

A. Nanoparticle binding dynamics

As the effects of membrane thermal undulations on the nanoparticle motion are brought out from the perspective of a locally fluctuating boundary, we first scrutinize the main characteristics of the nanoparticle dynamical relaxations when it is bound to a flat wall via different strengths of harmonic potential. This would also be a suitable reference system for which Eq. (9) applies with $z_m(t)$ fixed at $z = 0$. After reviewing the general features for the flat-wall system, detailed comparisons for the temporal correlation and spatial distribution functions of the NC center of mass are presented for different strengths of membrane bending rigidity.

As mentioned in Sec. III, the ACF of a given physical quantity characterizes how it correlates or decorrelates with its reference condition over time. For a bound NC, two dominant forces impact the transient relaxation of its velocity and position. As the typical Brownian motion of particle yields $v(t) \propto e^{-t/\tau_B}$, it is anticipated that the wall-mediated hydrodynamic resistance for the NC would first take place over the timescale of τ_B (or in the dimensionless form $\tau_B/\tau_v \sim 0.2$ for our case). Concurrently, the restraining effect due to the harmonic binding force would prevail over the timescale of τ_k. As demonstrated in Fig. 2(a), the particle velocity correlation initially decays at the timescale of τ_B followed by a transition to damped oscillations at the timescale of τ_k. The spike shown in the magnitude of VACF denotes the onset of anticorrelation as a result of the harmonic potential. Distinct from the wall-induced anticorrelation seen in the VACF for a particle moving in the direction perpendicular to the wall in the presence of fluid memory effect [71,72], the anticorrelation observed here is purely due to the oscillatory feature of a harmonically trapped particle [42–44]. For a binding constant k_b ranging from 1 to 0.01 N/m, it is clearly seen that the timescale at which anticorrelation maximizes (the first maximum following the spike) scales as $k_b^{-1/2}$. Moreover, a weaker harmonic spring constant leads to a smaller magnitude of anticorrelation. The close agreement between the results obtained from stochastic and deterministic simulations not only justify our methodology, but also suggests that the information of the velocity temporal response at long times
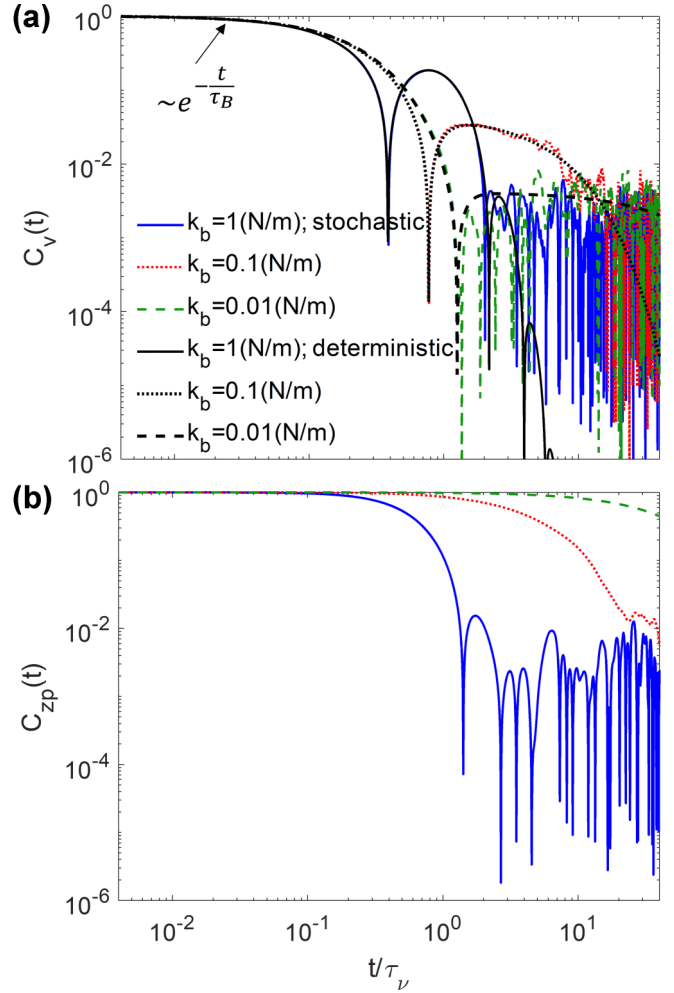

FIG. 2. (a) Normalized VACF as a function of the scaled time for an NC bound to a flat wall with varying harmonic force constant. The solutions from both stochastic LE (colored curves) and deterministic modeling (black curves) are shown for comparison. (b) The corresponding normalized PACF as a function of the scaled time for the NC. τ_v is the hydrodynamic viscous relaxation time.

($t > \tau_v$) may be gained from the deterministic method if satisfactory statistics is inaccessible in stochastic simulations. In Fig. 2(b), the temporal decay in the NC position fluctuations are consistent with the main features shown in the VACF. In general, a faster decay in the PACF is observed for a stronger nanoparticle binding potential, and the onset of decay appears at $t \sim \tau_k$ as the particle starts to decorrelate with its original configuration through oscillatory motion.

Once an NC is bound to a membrane surface, the temporal correlation of the membrane binding site would be altered from its force-free condition as shown in Fig. S1(a). As can be seen from the binding-site HACF of the membrane presented in Fig. 3, compared with the analytical expression for the HACF of a free membrane, $C_z(t) = \frac{\sum_{\mathbf{k}} k^{-4} e^{-\omega_{\mathbf{k}} t}}{\sum_{\mathbf{k}} k^{-4}}$ with $\omega_{\mathbf{k}} = K_c k^3/4\eta$, the membrane height shows a relaxation dynamics with a longer decaying timescale in the presence of binding, indicating that the pulling force from the NC makes the temporal correlation of membrane fluctuations more persistent. Comparing Figs. 3(a) and 3(b), the two insets show that a
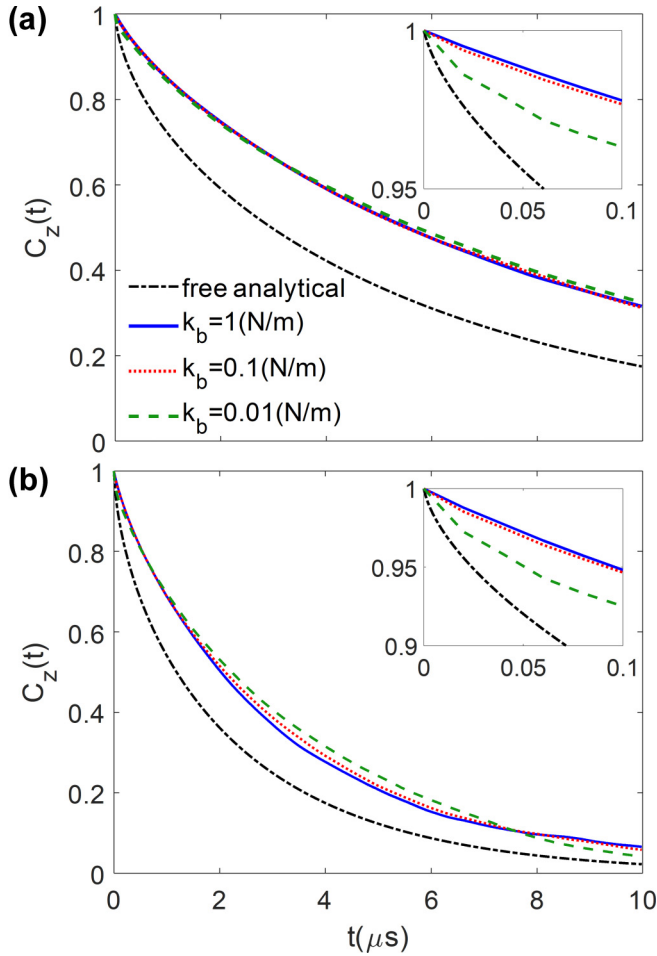
FIG. 3. Normalized membrane HACFs of the binding site as a function of time for varying binding spring constant compared to the analytical result for a free membrane. (a) $K_c = 20\ k_B T$ and (b) $K_c = 50\ k_B T$. The insets in (a) and (b) show the initial decay of the correlation functions.

slower initial decay in the binding site correlation function is observed for a stronger binding strength (k_b), suggesting a more substantial coupling to the dynamics of the bound nanoparticle. However, over longer times the HACFs depend on the binding strength in a more subtle way, and the decaying rate is nonmonotonic with k_b. We have also analyzed the HACF of the membrane grids neighboring to the binding site and found that in the presence of only monovalent interaction the effect of external binding is local and diminishes quickly away from the binding site. Consistent with this finding, the equal-time position correlation [see Fig. S1(b)] for the bound and free membranes are indistinguishable.

On the other hand, with regard to the NC adhesive dynamics, we first confirm that the Maxwell-Boltzmann distribution of velocity is obeyed. However, apparently the presence of an elastic fluid membrane modulates the oscillatory characteristics of velocity relaxation, as shown in Fig. 4. While the VACFs exhibit an initial decay of $\sim e^{-t/\tau_B}$ consistent with Fig. 2(a), the oscillatory correlation is generally suppressed by membrane undulations, and the effect is more substantial if the membrane is floppier with a smaller K_c. In fact, for
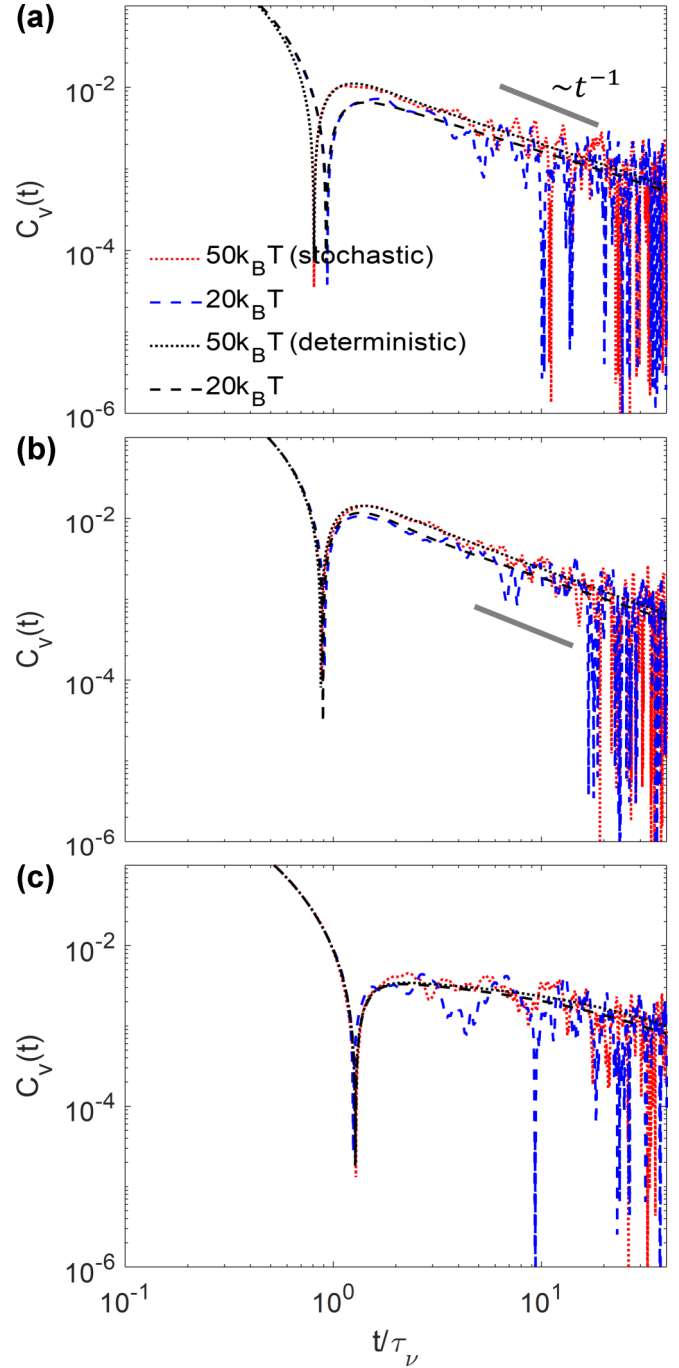

FIG. 4. Normalized VACFs as a function of the scaled time for an NC bound to a membrane of different values of bending rigidity at the binding force constant of (a) $k_b = 1$ N/m, (b) $k_b = 0.1$ N/m, and (c) $k_b = 0.01$ N/m. The stochastic simulations (colored lines) are compared with the velocity response function obtained from the deterministic method (black lines). τ_v is the hydrodynamic viscous relaxation time. The thick gray line in (a) and (b) denotes the scaling of t^{-1}.

stronger binding constants ($k_b > 0.1$ N/m), it is clearly seen in Figs. 4(a) and 4(b) that the oscillation in the presence of an undulating membrane changes to a more persistent anticorrelated long-time tail compared to the case with a flat, nonfluctuating surface presented in Fig. 2(a). From the complementary
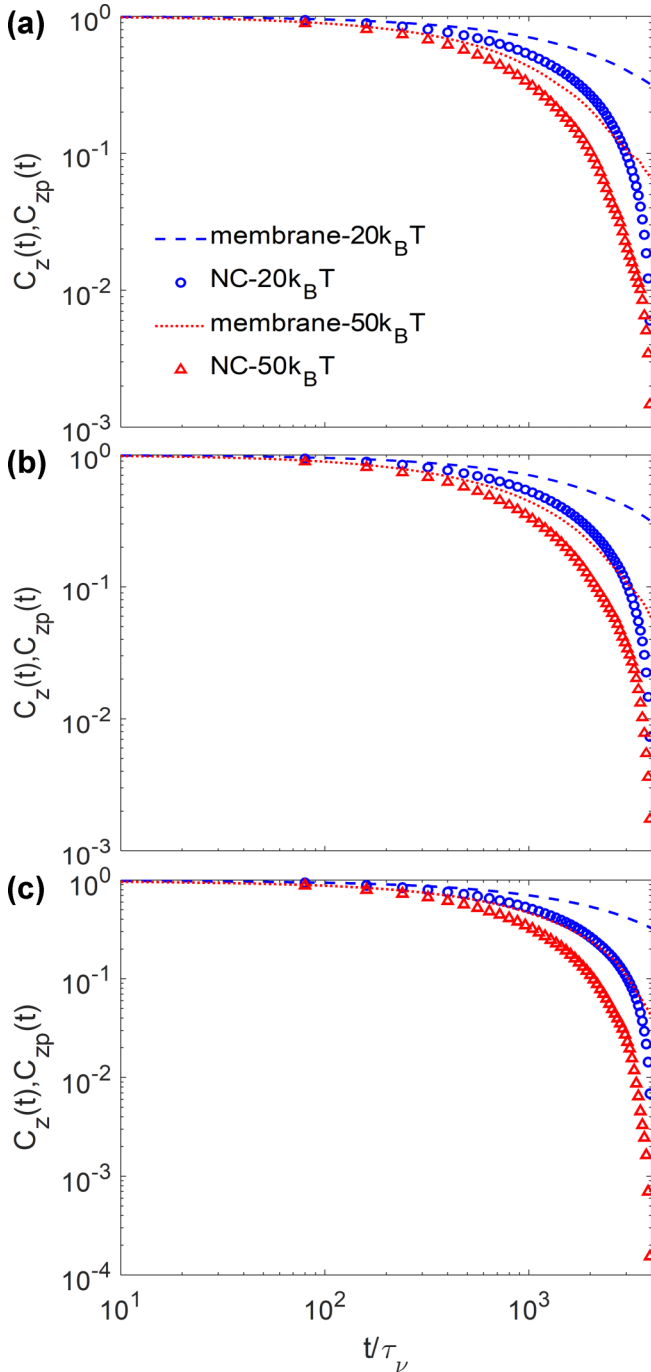
FIG. 5. Comparison between the NC PACFs and the membrane binding-site HACFs plotted as a function of the scaled time for different values of membrane bending rigidity at the binding force constant of (a) $k_b = 1$ N/m, (b) $k_b = 0.1$ N/m, and (c) $k_b = 0.01$ N/m. τ_ν is the hydrodynamic viscous relaxation time.

FIG. 6. Probability density distributions of ligand-receptor separation, d, for an NC bound to a membrane at $K_c = 20\,k_BT$ with three different binding force constants. Symbols are simulation results and lines are the corresponding Boltzmann distribution law, $\phi(d) \propto \exp\left(-\frac{k_b d^2}{2k_BT}\right)$.

in the presence of a softer adhesive potential as the particle may still have enough freedom to explore its conformational space, and the effect of an undulating boundary is negligible in the inertial regime at the timescale of τ_ν or τ_B.

While the NC VACF provides information about the dynamical relaxation in the inertial regime, its PACF may indicate the fluctuation correlation between the bound NC and membrane over longer times. In Fig. 5, we compare the NC PACFs side-by-side with the membrane binding-site HACFs for the parameter space considered in Fig. 4. Not surprisingly, the binding between NC and membrane makes their position variations highly coupled. Comparing the NC PACFs in this figure with the results in Fig. 2(b), apparently the long-time fluctuations of NC position are significantly suppressed and display a much longer memory in the presence of the relaxation of its interacting membrane binding site.

Aside from the temporal correlation between NC and membrane, it would be intriguing to investigate how the NC binding potential is impacted by membrane fluctuations. In Fig. 6, we first track the separation between the ligand and receptor (d) for various force constants at a membrane bending rigidity of $K_c = 20\,k_BT$. The distribution of d follows the Boltzmann distribution law set by each harmonic binding potential between the ligand and receptor. Such a close agreement between the simulated results and the theory further justifies our simulation protocol, and hydrodynamic fluctuations do not alter equilibrium distributions.

In Ref. [13], the NC binding PMF was characterized by defining an order parameter that quantifies the separation between the NC center of mass and the undulating membrane. Similarly in our one-dimensional setting, we define the order parameter ΔR based on the relative displacement of the centers of mass for the NC and the membrane elements falling between one diameter from NC (also see Sec. III). In Fig. 7, we compare the probability densities of ΔR, namely

deterministic solutions, we identify that the persistent decay approximately scales as t^{-1} in our simulation time frame. As the binding force constant decreases, the membrane-mediated damping effect becomes less significant. Eventually for $k_b = 0.01$ N/m, Fig. 4(c) shows that the VACFs for an NC bound to a flat wall [comparing to dashed lines in Fig. 2(a)] and an undulating membrane are very similar. This suggests that the coupled effect between membrane and nanoparticle is weaker
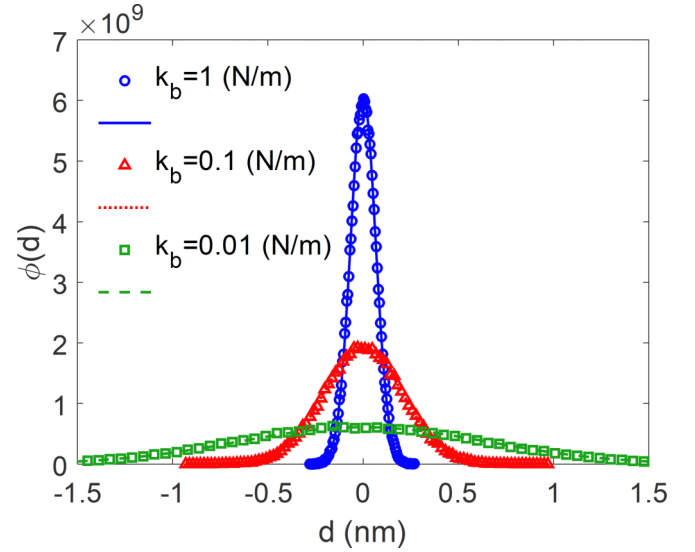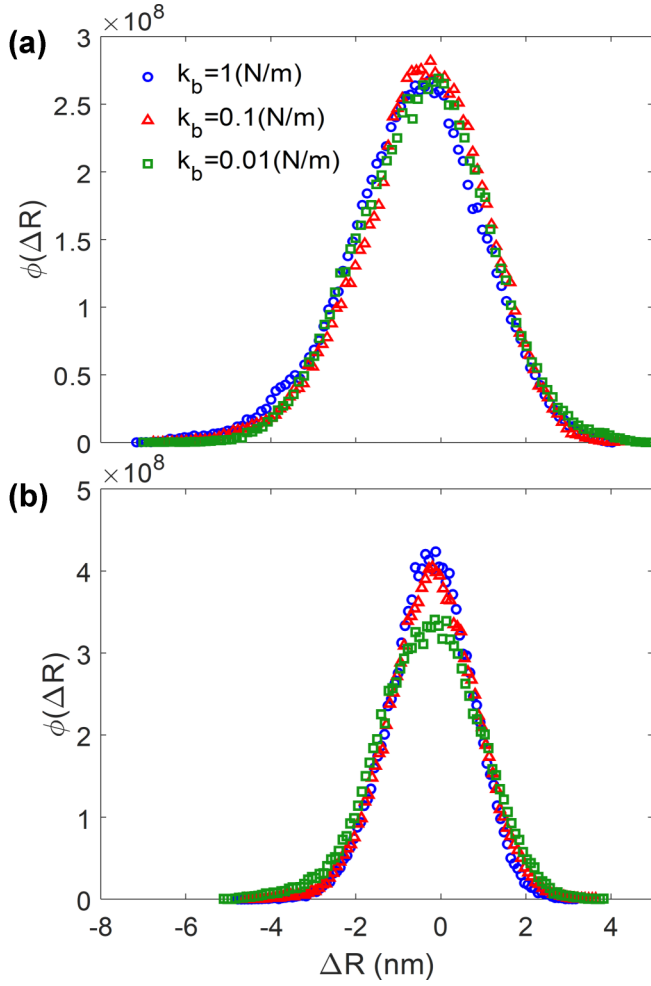
FIG. 7. Probability density distributions of the NC-membrane order parameter, $\Delta R = z_p - z_{c.m.}$ (see text), at various binding constants for (a) $K_c = 20 \, k_B T$ and (b) $K_c = 50 \, k_B T$.

$\phi(\Delta R)$, for different values of membrane bending rigidity and ligand-receptor binding strength. The corresponding

PMF for each case would be directly derived by calculating $-\ln \phi(\Delta R)$. First, it is apparent that the order parameter distribution function skews to the left ($\Delta R < 0$), indicating that the nanoparticle has a tendency to stay closer to the interacting membrane surface as a result of the ligand-receptor binding effect. Second, the width of the distribution function for ΔR is primarily dependent on the membrane stiffness, and a stiffer membrane (higher K_c value) leads to a narrower distribution and a higher maximum. For a given membrane stiffness, if the binding strength is weaker, the ΔR distribution is generally wider with a lower peak, an effect more prominent if K_c is higher. If we make a direct comparison between the distribution functions for ΔR and d at the same force constant k_b (Fig. 6 vs Fig. 7), it is noteworthy that the original harmonic binding energy landscape with a flat surface is smeared out by membrane fluidity, consistent with the observation in Ref. [13].

B. Barrier-crossing kinetics

So far, we have comprehensively explored the temporal correlations as well as the probability distributions for the degrees of freedom of the NC-membrane system. The focused time and length scales characterize the hydrodynamic response of NC coupled to membrane relaxation in the NC inertial regime. In this section, we demonstrate how the NC binding rate is impacted by an undulating membrane. In order to have a clear definition of the transition state between two specific bound states, we change the simple harmonic potential to a locally harmonic, bistable potential [53] shown in Fig. 8(a), where the bistable energy landscape shows two minimums with the lower one being the stable state (A) and the higher one being the metastable state (B). Such a double-well potential is motivated by the thermodynamically characterized one-dimensional potential of mean force for a ligand-functionalized nanoparticle multivalently bound to a receptor-expressing nonfluctuating surface [11,12]. Therefore, the two bound states could mimic the effective energy landscape of a multivalently bound NC [inset of Fig. 8(a)]. The shape of each bistable potential is defined based on the instantaneous ligand-receptor separation d by

$$F = \begin{cases} \frac{1}{2}k_b d^2, & \text{for } d \leqslant \frac{k_b^* d^*}{k_b^* + k_b} \\ F^* - \frac{1}{2}k_b^*(d - d^*)^2, & \text{for } \frac{k_b^* d^*}{k_b^* + k_b} < d \leqslant d^* + \sqrt{\frac{2k_b k_B T}{k_b^*(k_b + k_b^*)}} \\ F^* - k_B T + \frac{1}{2}k_b\left[d - d^* - \sqrt{\frac{2(k_b + k_b^*)k_B T}{k_b k_b^*}}\right], & \text{for } d > d^* + \sqrt{\frac{2k_b k_B T}{k_b^*(k_b + k_b^*)}} \end{cases}, \quad (11)$$

where F^* and d^* are the transition state energy and the transition state separation, respectively. As an example relevant for strong binding in vascular targeted drug delivery using antigen-functionalized NC, we fix $k_b = 1$ N/m in the following discussion. The invoked parameters are summarized in Table I. The shapes of the five potentials are chosen to separately elaborate the effects of the energy barrier (comparing potentials 1 to 3) and the transition state landscape (potentials 2 vs 4 and 3 vs 5). For the more diffuse transition state landscapes (potentials 4 and 5), $k_b^* = \frac{2k_b F^*}{k_b d^{*2} - 2F^*}$. We fix

the energy barrier for $B \rightarrow A$ as 1 $k_B T$ while allowing the energy barrier for $A \rightarrow B$ to vary.

Given the definition of the ligand-receptor binding transition state, the simulations are again performed in a two-stage process as mentioned in Sec. III. In order to increase the resolution in time, we choose $\Delta t_2 = 10^{-11}$ s and $N_2 = 5 \times 10^8$. For a prescribed bistable potential, once the membrane has equilibrated, at stage 2 an NC is placed to a distance corresponding to the potential minimum of one of the states above the membrane reference site (the binding site of receptor) with
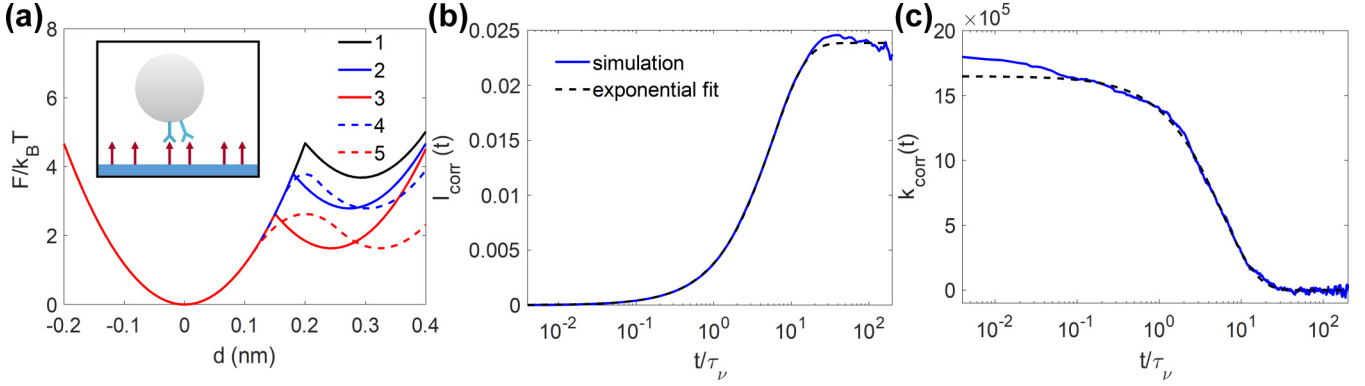
FIG. 8. (a) The ligand-receptor binding energy, F, as a function of the ligand-receptor separation, d, for the five bistable potentials defined by Eq. (11) and Table I. The inset schematic shows a functionalized nanoparticle multivalently bound to a receptor-expressing surface. (b) The time integral of the reactive flux correlation function, $I_{corr}^{A \to B}$, plotted as a function of the time scaled by the viscous relaxation time, τ_ν, for a ligand-functionalized nanoparticle bound to a receptor-expressing flat wall subjected to the binding landscape 1. The integral form of the exponential fit (explained in text) is shown. (c) The corresponding reactive flux correlation function, $k_{corr}^{A \to B}$, and the exponential fit in (b).

a zero initial velocity. We define a pair of characteristic state functions (h_A and h_B) in such a way that $h_A = 1$ and $h_B = 0$ for $d \leqslant d^*$, and $h_A = 0$ and $h_B = 1$ for $d > d^*$. Consequently, the time correlation function of the NC which is originally bound to state A, passes over the barrier at t with a given speed, and commit to state B is then determined by the reactive flux formalism [42,53,73], $k_{corr}^{A \to B}(t) \equiv \frac{\langle h_A[d(0)] \dot{h}_B[d(t)] \rangle}{\langle h_A[d(0)] \rangle}$. The reactive flux correlation function for the reverse reaction is defined as $k_{corr}^{B \to A}$ by switching the subscripts A and B. Instead of directly evaluating the speed passing over the barrier (which involves a time derivative in the ensemble average), we choose the time integral form of the correlation function to reduce the statistical error. In other words, we calculate $I_{corr}^{A \to B}(t) = \int_0^t k_{corr}^{A \to B}(t')dt' = \frac{\langle h_A[d(0)] h_B[d(t)] \rangle}{\langle h_A[d(0)] \rangle}$ and then take the time derivative with respect to it.

As a reference, we first perform simulations on the system without a fluctuating surface, i.e., a nanoparticle bound to a flat wall. In such a case, the ligand-receptor separation is directly determined by the displacement of the center of mass of nanoparticle in the z direction. In Figs. 8(b) and 8(c), the integral form of the reactive flux correlation function and the reactive flux correlation function itself are presented, respectively. In Fig. 8(b), $I_{corr}^{A \to B}(t)$ increases gradually and levels off; the corresponding $k_{corr}^{A \to B}(t)$ in Fig. 8(c) first shows an initial value (denoted as k_-^0) and decays over time. For the transition between the two states, $A \rightleftharpoons B$, it is straightforward to show that the macroscopic reaction rate for $A \to B$ is defined as an exponential function $k_- \exp(-t/\tau_{rxn})$. Here, τ_{rxn} is the characteristic reaction time which is related to the $A \to B$ and

$B \to A$ rate constants (k_- and k_+) via $\tau_{rxn}^{-1} = k_- + k_+$. Since the exponential decay for a Brownian particle is valid only after the short-time transient relaxation that couples to the hydrodynamics has finished [53], we fit $I_{corr}^{A \to B}(t)$ to the integral form of the exponential function, $k_- \tau_{rxn}[1 - \exp(-t/\tau_{rxn})]$, for $t > \tau_\nu$. In order to increase the accuracy, we perform variance-weighted least squares in our fitting and the standard errors of the results are generally within 1%. From the exponential fit in Fig. 8(c), it is clearly observed that $k_{corr}^{A \to B}(t)$ exhibits an exponential relaxation over long times. The deviation between the simulation and the exponential fit at short times indicates a transient behavior for barrier crossing over a timescale of $\tau_{mol} \sim \tau_\nu \ll \tau_{rxn}$ [53].

In the presence of a thermally fluctuating elastic membrane, we observe that the separation between the ligand and receptor crosses the energy barrier nearly immediately from state A given the narrow width of the bistable potential. As a result, the initial relaxation in the reactive flux correlation function displays a rapid drop over the timescale of just a few Δt_2, as seen in Fig. 9(b). According to the transition state theory [73], we may estimate the upper limit of the initial rate constant as $k_{-,max}^0 \sim k_-^{TST} = (1/\tau_{mol}) \exp(-\Delta F/k_B T)$ with $\Delta F = F^* - F_A$. Writing $\tau_{mol} \approx \Delta t_2$ leads to $k_{-,max}^0$ as high as 9×10^8 1/s for potential 1. Therefore, the rapid decrease shown in Fig. 9(b) at short times is roughly attributed to the immediate barrier crossing in our simulations. Given the continuum approximation invoked here, numerically reducing the time step size is expected to yield an even higher value of $k_{-,max}^0$, as shown in Fig. S5. We also note that $k_{corr}^{A \to B}(t)$ does not show a clear plateau regime defining the onset of the exponential decay. Therefore, we determine k_- and τ_{rxn} approximately by fitting $I_{corr}^{A \to B}(t)$ in Fig. 9(a) to the integral form of the exponential function for $t > 0.1\tau_\nu$, on the premise that k_- (or k_+) can still be determined as a constant.

Finally, in Fig. 10 we present the fitted parameters, k_- and $\tau_{rxn,-}$ (evaluated from $k_{corr}^{A \to B}$) as well as k_+ and $\tau_{rxn,+}$ (evaluated from $k_{corr}^{B \to A}$). The representative results for the NC-membrane system with $K_c = 50 k_B T$ are compared with the reference NC-wall system. As seen in Fig. 10(a) for k_- and Fig. 10(b) for k_+, for a given system the rate constants

TABLE I. Parameters for the five bistable potentials defined in Eq. (11).

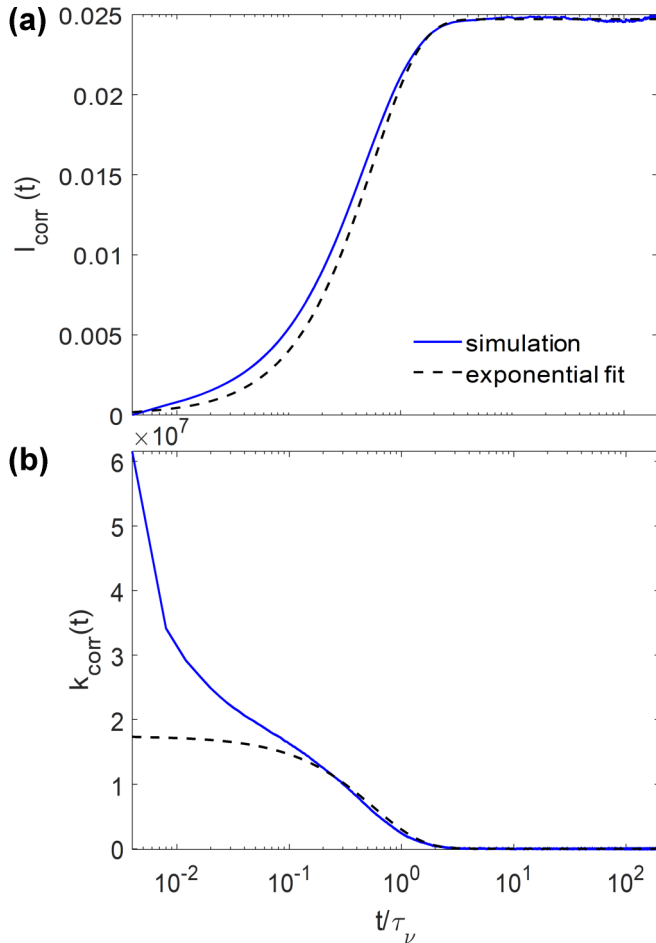| Potential	d^* (Å)	k_b^* (N/m)	F^* ($k_B T$)
1	2	100	4.68
2	1.8	100	3.79
3	1.5	100	2.63
4	2	4.26	3.79
5	2	1.29	2.63

FIG. 9. (a) The integral form of the reactive flux correlation function, $I_{corr}^{A \to B}$, plotted as a function of the time scaled by the viscous relaxation time, τ_ν, for a ligand-functionalized nanoparticle bound to a receptor-expressing membrane with $K_c = 50\ k_B T$ subjected to the binding landscape 1 [see Fig. 8(a)]. The exponential fit (explained in text) is shown. (b) The associated reactive flux correlation function, $k_{corr}^{A \to B}$, and the exponential fit in (a).

are affected not only by the energy barrier ΔF but also by the transition state landscape. Specifically, for either $A \to B$ or $B \to A$ reaction, although the ratio between the rate constants for any two potentials is roughly determined by the difference between the two energy barriers, the potential with a steeper transition state landscape generally shows a slightly higher rate, as the NC can pass over the barrier more quickly and commit to the other state. Furthermore, in both Figs. 10(a) and 10(b), apparently for a given potential the rate constant is augmented by about one order of magnitude in the presence of membrane fluctuations. In Fig. 10(c), the close agreement between the characteristic reaction time predicted from $k_{corr}^{A \to B}$ and that from $k_{corr}^{B \to A}$ justifies our chosen exponential fit for the mass action kinetics. Given the equilibrium constant for the reaction $B \rightleftharpoons A$ defined as $K_{eq} = k_+/k_-$ in our calculations, the ratio between K_{eq} for the NC-membrane system (at $K_c = 50\ k_B T$) and that for the NC-wall system varies from 0.66 to 0.88 for the five potentials. This suggests that an undulating surface may substantially facilitate the transition of a monovalently bound NC between two states
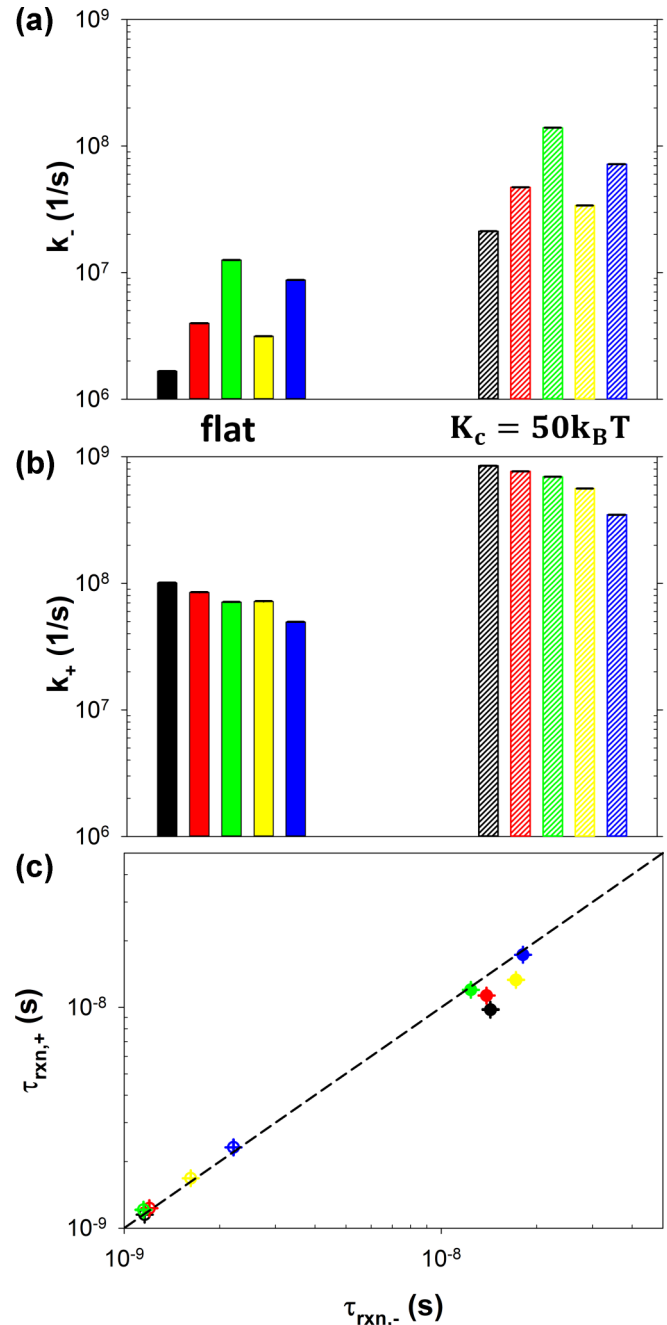

FIG. 10. Comparison of the predicted rate constants for (a) $A \to B$ reaction (k_-) and (b) $B \to A$ reaction (k_+) for the NC-wall system (left; filled bars) and the NC-membrane system (right; patterned bars) subjected to the five potentials. (c) Comparison of the time constants predicted from $A \to B$ reaction ($\tau_{rxn,-}$) and $B \to A$ reaction ($\tau_{rxn,+}$) for the NC-wall system (right; filled symbols) and the NC-membrane system (left; open symbols). The membrane has a fixed bending rigidity of 50 $k_B T$. Within each data group, the potentials 1–5 are consecutively shown in black, red, green, yellow, and blue.

without a significant change to the equilibrium constant. In the study of Hu *et al.* [9], fully three-dimensional dissipated particle dynamics simulations were performed to investigate the binding between membrane-anchored ligand and receptor proteins. It was found that the binding rate constant decreases

while the unbinding rate constant increases as the membrane shape fluctuations increase. Although our continuum model is simplistic with only one-dimensional motion of a bound NC that transitions between a metastable state B and a stable state A, the current results are qualitatively consistent with Hu *et al.* [9], and the slight decrease in the equilibrium constant with an undulating membrane may be attributed to the additional loss of the membrane entropy when a more stable ligand-receptor bond is formed.

V. CONCLUSIONS AND OUTLOOK

In this work, we have applied coupled Brownian dynamics equations to investigate the binding between a ligand-functionalized nanoparticle (or an NC) and a targeted receptor-expressing fluid membrane. By considering an effective, one-dimensional potential for monovalent binding between the nanoparticle and membrane, the current mesoscopic-continuum framework allows for the prediction of temporal correlations for the heights of membrane elements as well as the variations of nanoparticle center-of-mass velocity and position along with the associated equilibrium probability distributions. Moreover, the simulated trajectories of the instantaneous separation between the surface-anchored ligand and receptor subjected to a bistable potential have been analyzed to yield the reactive flux correlation function for the NC passing over an energy barrier distinguishing two bound states. We have found that when the NC is bound to an undulating membrane, the harmonic-force-driven oscillatory behavior of the NC velocity autocorrelation is substantially suppressed, and the corresponding NC position fluctuations are coupled to the out-of-plane motion of the membrane binding site, thus yielding longer correlation times for the dynamics of both NC and membrane. From the distribution of the NC relative to the center-of-mass of the representative membrane elements, the binding potential of mean force is impacted by the softness of the membrane, and the softer the membrane (with a lower bending rigidity) the broader and shallower the potential landscape. Finally, with respect to the transition kinetics of a bound NC between two wells of a bistable potential with varying transition state conditions, we have also discovered that the transition rate of the NC is primarily dependent on its capability of exploring the configurational space within the bistable potential. As a result, it is not surprising that the rate constant is increased in the presence of an undulating fluid membrane as more fluctuations are associated with the NC position.

The chosen radius of the nanoparticle in this study is primarily motivated by targeted drug delivery applications where the optimal size of the NC is about tens to hundreds of nanometers [10–13]. However, in other context-specific applications different sizes of nanoparticles may be relevant. Given the hydrodynamic scaling in our theory, the features seen in the autocorrection functions presented as a function of the time scaled by the hydrodynamic viscous relaxation time ($\tau_v \propto a^2$) for a nanoparticle of different size would remain qualitatively the same with variations dependent on the relative scales of Brownian relaxation time ($\tau_B \propto a^2$) and harmonic-spring oscillation time for the binding interaction ($\tau_k \propto a^{\frac{3}{2}}$). Moreover, given the viscous drag force ($\sim -6\pi\mu a \frac{dz_p}{dt}$) and the spring force ($\sim -k_b z_p$) appearing in the nanoparticle equation of motion, another timescale characterizing the balance between these two forces would be $\tau_c = \frac{6\pi\mu a}{k_b} \propto a$ [53]. Consequently, the predicted variation of the transition rate constants with the particle radius would be bounded by the two scaling laws of τ_k^{-1} and τ_c^{-1}, respectively, provided the binding strength and other fluctuating effects remain unchanged. Therefore, changing the size of the particle by one order of magnitude would roughly result in a rate constant varied by a factor of 10 to 30.

In the present coarse-grained framework, we have bridged the essential physics of nanoparticle near-wall hydrodynamic resistance and membrane shape fluctuations subjected to thermodynamic descriptions for the ligand-receptor binding as well as the membrane elastic Hamiltonian. We have shown that our results agree qualitatively with previous studies using more detailed membrane models with the predicted features being in agreement with relevant biological conditions [9,13]. In a multiscale and multiphysics problem such as the one presented here, efficient and straightforward characterization for the spatial-temporal correlations in the fluid inertial regime is only possible by a unified computational model that suitably takes into account all the relevant degrees of freedom involved. Given the quasisteady assumption for the nearmembrane lubrication force, the characterized microscopic correlation functions provide an unambiguous connection with the macroscopic measurables, as clearly demonstrated in our analyses of the apparent rate constant for the nanoparticle. It is also anticipated that the one-dimensional binding potential would be a minimal representation of an effective energy landscape along the "reaction coordinate" of interest. More detailed shapes of the potential with a spatially varied force constant could be employed in the general methodology presented in this work to gain insights into the binding of functionalized nanoparticles in a variety of biophysical conditions.

[1] M. Schulz, A. Olubummo, and W. H. Binder, Beyond the lipid-bilayer: Interaction of polymers and nanoparticles with membranes, Soft Matter **8**, 4849 (2012).

[2] C. Contini, M. Schneemilch, S. Gaisford, and N. Quirke, Nanoparticle-membrane interactions, J. Exp. Nanosci. **13**, 62 (2018).

[3] E. S. Melby, C. Allen, I. U. Foreman-Ortiz, E. R. Caudill, T. R. Kuech, A. M. Vartanian, X. Zhang, C. J. Murphy, R. Hernandez, and J. A. Pedersen, Peripheral membrane proteins facilitate nanoparticle binding at lipid bilayer interfaces, Langmuir **34**, 10793 (2018).

[4] T. Osaki and S. Takeuchi, Artificial cell membrane systems for biosensing applications, Anal. Chem. **89**, 216 (2017).

[5] N. Misawa, T. Osaki, and S. Takeuchi, Membrane protein-based biosensors, J. Royal Soc. Interface **15**, 20170952 (2018).

[6] E. Barbieri, P. P. Di Fiore, and S. Sigismund, Endocytic control of signaling at the plasma membrane, Curr. Opin. Cell Biol. **39**, 21 (2016).

[7] V. Haucke and M. M. Kozlov, Membrane remodeling in clathrin-mediated endocytosis, J. Cell Sci. **131**, jcs216812 (2018).

[8] C. R. Hauck, Cell adhesion receptors—Signaling capacity and exploitation by bacterial pathogens, Med. Microbiol. Immunol. **191**, 55 (2002).

[9] J. Hu, R. Lipowsky, and T. R. Weikl, Binding constants of membrane-anchored receptors and ligands depend strongly on the nanoscale roughness of membranes, Proc. Natl. Acad. Sci. USA **110**, 15283 (2013).

[10] N. J. Agrawal and R. Radhakrishnan, The role of glycocalyx in nanocarrier-cell adhesion investigated using a thermodynamic model and Monte Carlo simulations, J. Phys. Chem. C **111**, 15848 (2007).

[11] J. Liu, G. E. Weller, B. Zern, P. S. Ayyaswamy, D. M. Eckmann, V. R. Muzykantov, and R. Radhakrishnan, Computational model for nanocarrier binding to endothelium validated using in vivo, in vitro, and atomic force microscopy experiments, Proc. Natl. Acad. Sci. USA **107**, 16530 (2010).

[12] B. J. Zern, A.-M. Chacko, J. Liu, C. F. Greineder, E. R. Blankemeyer, R. Radhakrishnan, and V. Muzykantov, Reduction of nanoparticle avidity enhances the selectivity of vascular targeting and PET detection of pulmonary inflammation, ACS Nano **7**, 2461 (2013).

[13] N. Ramakrishnan, R. W. Tourdot, D. M. Eckmann, P. S. Ayyaswamy, V. R. Muzykantov, and R. Radhakrishnan, Bio-physically inspired model for functionalized nanocarrier adhesion to cell surface: Roles of protein expression and mechanical factors, Royal Soc. Open Sci. **3**, 160260 (2016).

[14] G. J. Doherty and H. T. McMahon, Mechanisms of endocytosis, Annu. Rev. Biochem. **78**, 857 (2009).

[15] M. Kaksonen and A. Roux, Mechanisms of clathrin-mediated endocytosis, Nat. Rev. Mol. Cell Biol. **19**, 313 (2018).

[16] J. Zimmerberg and M. M. Kozlov, How proteins produce cellular membrane curvature, Nat. Rev. Mol. Cell Biol. **7**, 9 (2006).

[17] W. Helfrich, Elastic properties of lipid bilayers: Theory and possible experiments, Z. Naturforsch. C **28**, 693 (1973).

[18] R. Lipowsky, The conformation of membranes, Nature **349**, 475 (1991).

[19] T. Curk, P. Wirnsberger, J. Dobnikar, D. Frenkel, and A. Šarić, Controlling cargo trafficking in multicomponent membranes, Nano Lett. **18**, 5350 (2018).

[20] M. Deserno, Elastic deformation of a fluid membrane upon colloid binding, Phys. Rev. E **69**, 031903 (2004).

[21] X. Yi, X. Shi, and H. Gao, Cellular Uptake of Elastic Nanoparticles, Phys. Rev. Lett. **107**, 098101 (2011).

[22] S. Dasgupta, T. Auth, and G. Gompper, Wrapping of ellipsoidal nano-particles by fluid membranes, Soft Matter **9**, 5473 (2013).

[23] R. Vácha, F. J. Martinez-Veracoechea, and D. Frenkel, Receptor-mediated endocytosis of nanoparticles of various shapes, Nano Lett. **11**, 5391 (2011).

[24] R. Vácha, F. J. Martinez-Veracoechea, and D. Frenkel, Intra-cellular release of endocytosed nanoparticles upon a change of ligand receptor interaction, ACS Nano **6**, 10598 (2012).

[25] A. H. Bahrami, Orientational changes and impaired internal-ization of ellipsoidal nanoparticles by vesicle membranes, Soft Matter **9**, 8642 (2013).

[26] A. H. Bahrami, R. Lipowsky, and T. R. Weikl, Tubulation and Aggregation of Spherical Nanoparticles Adsorbed on Vesicles, Phys. Rev. Lett. **109**, 188102 (2012).

[27] A. Šarić and A. Cacciuto, Mechanism of Membrane Tube Formation Induced by Adhesive Nanocomponents, Phys. Rev. Lett. **109**, 188101 (2012).

[28] C. van der Wel, A. Vahid, A. Šarić, T. Idema, D. Heinrich, and D. J. Kraft, Lipid membrane-mediated attraction between curvature inducing objects, Sci. Rep. **6**, 32825 (2016).

[29] H. Brenner, The slow motion of a sphere through a viscous fluid towards a plane surface, Chem. Eng. Sci. **16**, 242 (1961).

[30] A. J. Goldman, R. G. Cox, and H. Brenner, Slow viscous motion of a sphere parallel to a plane wall. i. motion through a quiescent fluid, Chem. Eng. Sci. **22**, 637 (1967).

[31] A. J. Goldman, R. G. Cox, and H. Brenner, Slow viscous motion of a sphere parallel to a plane wall. 2. couette flow, Chem. Eng. Sci. **22**, 653 (1967).

[32] R. G. Cox and H. Brenner, Slow motion of a sphere through a viscous fluid towards a plane surface. 2. small gap widths including inertial effects, Chem. Eng. Sci. **22**, 1753 (1967).

[33] S. H. Lee, R. S. Chadwick, and L. G. Leal, Motion of a sphere in the presence of a plane interface. 1. Approximate solution by generalization of the method of Lorentz, J. Fluid Mech. **93**, 705 (1979).

[34] S. H. Lee and L. G. Leal, Motion of a sphere in the presence of a plane interface. 2. An exact solution in bipolar coordinates, J. Fluid Mech. **98**, 193 (1980).

[35] S. H. Lee and L. G. Leal, The motion of a sphere in the presence of a deformable interface. 2. A numerical study of the translation of a sphere normal to an interface, J. Colloid Interf. Sci. **87**, 81 (1982).

[36] C. Berdan and L. G. Leal, Motion of a sphere in the presence of a deformable interface. 1. perturbation of the interface from flat—The effects on drag and torque, J. Colloid Interf. Sci. **87**, 62 (1982).

[37] T. Bickel, Brownian motion near a liquid-like membrane, Eur. Phys. J. E **20**, 379 (2006).

[38] B. U. Felderhof, Effect of surface tension and surface elas-ticity of a fluid-fluid interface on the motion of a particle immersed near the interface, J. Chem. Phys. **125**, 144718 (2006).

[39] T. Bickel, Hindered mobility of a particle near a soft interface, Phys. Rev. E **75**, 041403 (2007).

[40] A. Daddi-Moussa-Ider and S. Gekle, Hydrodynamic interaction between particles near elastic interfaces, J. Chem. Phys. **145**, 014905 (2016).

[41] A. Daddi-Moussa-Ider and S. Gekle, Brownian motion near an elastic cell membrane: A theoretical study, Eur. Phys. J. E **41**, 19 (2018).

[42] H.-Y. Yu, D. M. Eckmann, P. S. Ayyaswamy, and R. Radhakrishnan, Composite generalized Langevin equation for Brownian motion in different hydrodynamic and adhesion regimes, Phys. Rev. E **91**, 052303 (2015).

[43] H. Vitoshkin, H.-Y. Yu, D. M. Eckmann, P. S. Ayyaswamy, and R. Radhakrishnan, Nanoparticle stochastic motion in the inertial regime and hydrodynamic interactions close to a cylindrical wall, Phys. Rev. Fluids **1**, 054104 (2016).

[44] Y.-W. Wu and H.-Y. Yu, Adhesion of a polymer-grafted nanoparticle to cells explored using generalized Langevin dynamics, Soft Matter **14**, 9910 (2018).

[45] R. Granek, From semi-flexible polymers to membranes: Anomalous diffusion and reptation, J. Phys. II France **7**, 1761 (1997).

[46] Lawrence C.-L. Lin and F. L. H. Brown, Brownian Dynamics in Fourier Space: Membrane Simulations Over Long Length and Time Scales, Phys. Rev. Lett. **93**, 256001 (2004).

[47] Lawrence C.-L. Lin and F. L. H. Brown, Dynamic simulations of membranes with cytoskeletal interactions, Phys. Rev. E **72**, 011910 (2005).

[48] A. Naji and F. L. H. Brown, Diffusion on ruffled membrane surfaces, J. Chem. Phys. **126**, 235103 (2007).

[49] E. Reister-Gottfried, S. M. Leitenberger, and U. Seifert, Hybrid simulations of lateral diffusion in fluctuating membranes, Phys. Rev. E **75**, 011908 (2007).

[50] E. Reister-Gottfried, S. M. Leitenberger, and U. Seifert, Diffusing proteins on a fluctuating membrane: Analytical theory and simulations, Phys. Rev. E **81**, 031903 (2010).

[51] E. Reister, T. Bihr, U. Seifert, and A.-S. Smith, Two intertwined facets of adherent membranes: Membrane roughness and correlations between ligand-receptors bonds, New J. Phys. **13**, 025003 (2011).

[52] B. Marzban and H. Yuan, The effect of thermal fluctuation on the receptor-mediated adhesion of a cell membrane to an elastic substrate, Membranes **7**, 24 (2017).

[53] H.-Y. Yu, D. M. Eckmann, P. S. Ayyaswamy, and R. Radhakrishnan, Effect of wall-mediated hydrodynamic fluctuations on the kinetics of a Brownian nanoparticle, Proc. R. Soc. A **472**, 20160397 (2016).

[54] R. Singh and J. W. Lillard, Nanoparticle-based targeted drug delivery, Exp. Molec. Pathol. **86**, 215 (2009).

[55] J. Nicolas, S. Mura, D. Brambilla, N. Mackiewicz, and P. Couvreur, Design, functionalization strategies and biomedical applications of targeted biodegradable/biocompatible polymer-based nanocarriers for drug delivery, Chem. Soc. Rev. **42**, 1147 (2013).

[56] K. P. Garcia, K. Zarschler, L. Barbaro, J. A. Barreto, W. O'Malley, L. Spiccia, H. Stephan, and B. Graham, Zwitterionic-coated "stealth" nanoparticles for biomedical applications: Recent advances in countering biomolecular corona formation and uptake by the mononuclear phagocyte system, Small **10**, 2516 (2014).

[57] D. Grillo, M. O. de la Cruz, and I. Szleifer, Theoretical studies of the phase behavior of DPPC bilayers in the presence of macroions, Soft Matter **7**, 4672 (2011).

[58] R. J. Nap and I. Szleifer, How to optimize binding of coated nanoparticles: Coupling of physical interactions, molecular organization and chemical state, Biomater. Sci. **1**, 814 (2013).

[59] S. Wang and E. E. Dormidontova, Nanoparticle design optimization for enhanced targeting: Monte Carlo simulations, Biomacromolecules **11**, 1785 (2010).

[60] S. Wang and E. E. Dormidontova, Nanoparticle targeting using multivalent ligands: Computer modeling, Soft Matter **7**, 4435 (2011).

[61] S. Wang and E. E. Dormidontova, Selectivity of Ligand-Receptor Interactions Between Nanoparticle and Cell Surfaces, Phys. Rev. Lett. **109**, 238102 (2012).

[62] N. J. Agrawal and R. Radhakrishnan, Calculation of free energies in fluid membranes subject to heterogeneous curvature fields, Phys. Rev. E **80**, 011925 (2009).

[63] R. Radhakrishnan, B. Uma, J. Liu, P. S. Ayyaswamy, and D. M. Eckmann, Temporal multiscale approach for nanocarrier motion with simultaneous adhesion and hydrodynamic interactions in targeted drug delivery, J. Comp. Phys. **244**, 252 (2013).

[64] R. Kubo, The fluctuation-dissipation theorem, Rep. Prog. Phys. **29**, 255 (1966).

[65] See Supplemental Material at http://link.aps.org/supplemental/10.1103/PhysRevE.101.032604 for computational results for validation: free membrane correlations, nanoparticle-wall statistics, system size effects, and time step discussion.

[66] D. Frenkel and B. Smit, *Understanding Molecular Simulation: From Algorithms to Applications*, Vol. 1 (Elsevier, Amsterdam, 2001).

[67] C. Monzel and K. Sengupta, Measuring shape fluctuations in biological membranes, J. Phys. D: Appl. Phys. **49**, 243002 (2016).

[68] A. Biswas, A. Alex, and B. Sinha, Mapping cell membrane fluctuations reveals their active regulation and transient heterogeneities, Biophys. J. **113**, 1768 (2017).

[69] T. Betz and C. Sykes, Time resolved membrane fluctuation spectroscopy, Soft Matter **8**, 5317 (2012).

[70] F. Valentino, P. Sens, J. Lemière, A. Allard, T. Betz, C. Campillo, and C. Sykes, Fluctuations of a membrane nanotube revealed by high-resolution force measurements, Soft Matter **12**, 9429 (2016).

[71] B. Felderhof, Effect of the wall on the velocity autocorrelation function and long-time tail of Brownian motion, J. Phys. Chem. B **109**, 21406 (2005).

[72] T. Franosch and S. Jeney, Persistent correlation of constrained colloidal motion, Phys. Rev. E **79**, 031402 (2009).

[73] D. Chandler, *Introduction to Modern Statistical Mechanics* (Oxford University Press, New York, 1987).